Measuring the nonseparability of vector vortex beams

Melanie McLaren,[1] Thomas Konrad,[2] and Andrew Forbes[1,3,*]

[1]*School of Physics, University of the Witwatersrand, Johannesburg 2000, South Africa*
[2]*School of Chemistry and Physics, University of Kwazulu-Natal, Private Bag X54001, Durban 4000, South Africa*
[3]*CSIR National Laser Centre, P.O. Box 395, Pretoria 0001, South Africa*

Vector beams have the defining property of nonseparable spatial and polarization degrees of freedom and are now routinely generated in the laboratory and used in a myriad of applications. Here we exploit the nonseparability of such beams, akin to entanglement of quantum states, to apply tools traditionally associated with quantum measurements to these classical fields. We find that the entanglement entropy is a proxy for the average degree of polarization and thus provides a single number for the vector nature of such beams. In addition to providing tools for the analysis of vector beams, we also explore the concept of classical entanglement to explain why these tools are appropriate in the first place.

I. INTRODUCTION

Light beams with spatially inhomogeneous states of polarization, referred to as vector beams, have recently received increased interest in a variety of fields [1,2]. In particular, cylindrically symmetric vector (CV) beams have the ability to produce tighter focal spots with strong field gradients [3,4], finding applications in microscopy [5,6], interferometry [2], and optical tweezing [7]. CV modes have been observed in laser resonators [8,9] and optical fibers [10,11] and have more recently been generated by liquid-crystal displays [12], interferometric techniques [13], and q plates [14–16]. More general higher-order Poincaré sphere beams are the natural modes of many fibers [17,18]. A key characteristic of such vector fields is the coupling between the polarization and the spatial mode: in contrast to scalar fields, these degrees of freedom (DOF) are nonseparable, as depicted graphically in Fig. 1. These nonseparable DOF have been shown to improve upon existing techniques such as polarization metrology [19].

Despite the coupling of the polarization and spatial modes, the existing methods of measuring vector beams do so by treating these DOF independently. For example, there has been a great deal of work in determining the spatial mode content of a beam, e.g., modal interference [20], phase-retrieval algorithms [21,22], and modal decomposition by digital holograms [23,24]. Meanwhile the state of polarization of a beam is commonly measured using Stokes polarimetry with which, at each point of the beam, the polarization orientation and ellipticity can be calculated [25]. This versatile tool has been used for the real-time monitoring of optical wave fronts during propagation [26] and for studying topological structures of polarization in vector vortex beams [16].

Here we employed measurement techniques more commonly associated with quantum entanglement experiments to determine the degree to which a vector beam is nonseparable in spatial mode and polarization, in other words, the degree of the vector nature of the field. Our hypothesis is that since nonseparability is not unique to quantum mechanics, many of the tools for measuring this must be applicable to vector beams too. We employ ubiquitous quantum tools to differentiate

---

*Corresponding author: andrew.forbes@wits.ac.za

between scalar and vector beams: a Bell-type inequality measurement [27], a concurrence measurement [28], and an entanglement entropy measurement [29]. We show that the former indicates if an unknown field is vector in nature, while the two other measurements allow the degree to which the field is vectorial to be measured, with a range from 0 (fully scalar) to 1 (fully vector). Bell measurements have been performed on vector beams to illustrate a classical equivalent of spin-orbit hybrid quantum entanglement [30,31] and have been utilized in classical optical coherence as a quantitative characterization technique [32]. Both the linear entropy [33] and the Schmidt rank [34] have been suggested as measures of classical nonseparability. Here we offer tools to determine the degree of the vector nature of an unknown field. We also discuss the implications of these findings for mimicking quantum processes with classical states of light, in which the direction of the corresponding electric field on a transversal plane is not homogeneous, forming an example of so-called classically entangled light [35,36].

II. THEORY

We first derive a measure for the degree of the vector nature of coherent paraxial beams and then for the more general case of incoherent mixtures of paraxial beams. To begin, let us consider a paraxial vector beam with frequency ω propagating along the z axis, as represented by a complex-valued electric field $\mathbf{E} = E_0 e^{i\omega t}\mathbf{\Psi}$ with a unit-amplitude complex vector field

$$\mathbf{\Psi}(r,\phi,z) = \sqrt{a}\,u_R(r,\phi,z)\hat{\mathbf{e}}_R + \sqrt{(1-a)}\,u_L(r,\phi,z)\hat{\mathbf{e}}_L, \quad (1)$$

where a determines the relative weighting of fields u_R and u_L, which are normalized (i.e., $\int |u_{R,L}|^2 r\,dr\,d\phi = 1$) and specify the spatial dependence of the right-handed and left-handed circular polarization components associated with the canonical basis vectors $\hat{\mathbf{e}}_R$ and $\hat{\mathbf{e}}_L$.

We can rewrite Eq. (1) in bra-ket notation [37] as

$$|\Psi\rangle = \sqrt{a}|u_R\rangle \otimes |R\rangle + \sqrt{(1-a)}|u_L\rangle \otimes |L\rangle, \quad (2)$$

where the kets $|u_R\rangle,|u_L\rangle$ are unit vectors in an infinite-dimensional Hilbert space $\mathcal{H}_\infty$ representing the complex spatial fields on a transversal plane (the corresponding parameter z is omitted) and $|R\rangle,|L\rangle \in \mathcal{H}_2$ stand for the right-handed and
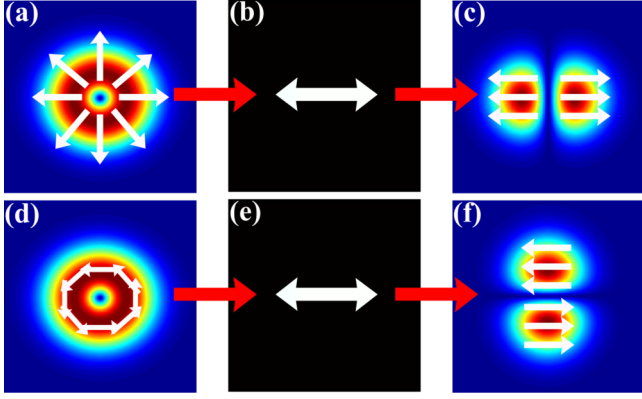
FIG. 1. (Color online) Schematic showing the spatial dependency of a vector beam on the polarization state. (a) A radially polarized vector beam incident on (b) a polarizer orientated to transmit horizontally polarized light produces (c) two petals orientated along the horizontal axis. (d) An azimuthally polarized vector beam incident on (e) a polarizer orientated to transmit horizontally polarized light produces (f) two petals orientated along the vertical axis.

the left-handed circular polarization vectors, respectively. The symbol $\otimes$ denotes the tensor product between the vectors. In quantum mechanics a state $|\Psi\rangle$ of the form in Eq. (2) is called nonseparable or entangled if it cannot be written as a product of any two vectors $|u\rangle \in \mathcal{H}_\infty$ and $|P\rangle \in \mathcal{H}_2$, i.e., $|\Psi\rangle \neq |u\rangle \otimes |P\rangle$. The nonseparability of the state $|\Psi\rangle$ thus exactly matches the definition of a vector beam as a beam with varying polarization over a transversal plane; that is, **E** cannot be written as a product of a scalar field and a polarization vector, which implies the nonseparability of the state vector $|\Psi\rangle$ and hence, formally, its entanglement.

Therefore, measures of entanglement for quantum systems can be employed to measure the degree of the vector nature of a vector beam. For example, when $a = 1/2$ and the two modes $|u_R\rangle$ and $|u_L\rangle$ are orthogonal, the field is purely vector (a maximally entangled state), whereas when $a = 0$ or 1 or the modes are the same, the field is purely scalar (a product state).

What is the best-suited entanglement measure in order to define the vector nature? For pure states of bipartite quantum systems there is a fundamental entanglement measure on which most operational measures are based, the entanglement entropy [29]. Consider a two-partite state $|\Psi\rangle \in \mathcal{H}_\infty \otimes \mathcal{H}_2$ as used to describe the state of a paraxial beam. The entanglement entropy is then given by the von Neumann entropy of the reduced density matrix of one of the subsystems, for instance, the polarization P, which is obtained by tracing over the spatial degree of freedom S:

$$E(|\Psi\rangle) = -\mathrm{Tr}[\rho_P \log(\rho_P)], \quad \rho_P = \mathrm{Tr}_S[|\Psi\rangle\langle\Psi|]. \quad (3)$$

In order to understand the physical meaning of these operations in our optical context, we first note that the density matrix ρ of $|\Psi\rangle\langle\Psi|$ expressed with respect to the polarization basis $|R\rangle, |L\rangle$,

$$\rho = \begin{pmatrix} a|u_R\rangle\langle u_R| & \sqrt{a(1-a)}|u_R\rangle\langle u_L| \\ \sqrt{a(1-a)}|u_L\rangle\langle u_R| & (1-a)|u_L\rangle\langle u_L| \end{pmatrix}, \quad (4)$$

corresponds to the beam coherence-polarization matrix [38], which represents the state of light of vector beams. Averaging (tracing) ρ over the spatial degree of freedom with an arbitrary set of orthonormal basis modes $|b_i\rangle$, we obtain a matrix that resembles a polarization (or coherency) matrix [32,39] as usually defined for scalar beams:

$$\rho_P = \sum_i \begin{pmatrix} a\langle b_i|u_R\rangle\langle u_R|b_i\rangle & \sqrt{a(1-a)}\langle b_i|u_R\rangle\langle u_L|b_i\rangle \\ \sqrt{a(1-a)}\langle b_i|u_L\rangle\langle u_R|b_i\rangle & (1-a)\langle b_i|u_L\rangle\langle u_L|b_i\rangle \end{pmatrix} \quad (5)$$

$$= \begin{pmatrix} a & \sqrt{a(1-a)}\langle u_L|u_R\rangle \\ \sqrt{a(1-a)}\langle u_R|u_L\rangle & (1-a) \end{pmatrix}. \quad (6)$$

However, the vector-beam equivalent of the polarization matrix for scalar beams can be argued to be the local polarization matrix $\tilde{\rho}(r,\phi,z) = \begin{pmatrix} |u_R|^2 & u_R u_L^* \\ u_L u_R^* & |u_L|^2 \end{pmatrix}$, where each matrix element depends on the spatial coordinates r, ϕ, z, and defines in this way the polarization properties of the beam in each point in space [38]. On the other hand, the reduced density matrix ρ_P determines the *average* polarization of the vector beam. It can be detected, for example, by measuring the components $s_i = \mathrm{Tr}[\sigma_i \rho_P]$ of the Bloch vector **s** with $\rho_P = (\mathbb{I} + \sum_i s_i \sigma_i)/2$, which correspond to the Stokes parameters. Here $i = 1,2,3$ and the Pauli operators σ_i are given by $\sigma_1 = |H\rangle\langle H| - |V\rangle\langle V|$, $\sigma_2 = \frac{1}{2}(|H + V\rangle\langle H + V| - |H - V\rangle\langle H - V|)$, and $\sigma_3 = |R\rangle\langle R| - |L\rangle\langle L|$. This is done, e.g., by means of polarization filters that cover the full beam cross section and integrating the total beam intensity after the filters. Alternatively, the total beam intensity after the filters can be determined by detecting and integrating the modal weights

$|\langle b_i|u_{R,L}\rangle|^2$ [Eq. (5)] with respect to any basis set of spatial modes $|b_i\rangle$. We discuss the application of such a modal decomposition technique below. Since the reduced density matrix ρ_P [Eq. (6)] describes the state of polarization averaged over a transversal plane, in general, it resembles the polarization matrix of an incoherent mixture, even though the vector beam including the spatial dependence is characterized by a coherent superposition $|\Psi\rangle$. Only in the extreme case of a beam with homogeneous polarization $|P\rangle$, i.e., for a scalar beam, does the reduced density matrix reflect a pure state, $\rho_P = |P\rangle\langle P|$. For vector beams, ρ_P can be written as a mixture of pure states: $\rho_P = \sum_i p_i |P_i\rangle\langle P_i|$. The entanglement can thus be quantified in terms of the "mixedness" of ρ_P as given by the von Neumann entropy [see Eq. (3)]. The latter yields the Shannon entropy of the statistical weights p_i of a decomposition of ρ_P with respect to orthonormal states $|P_i\rangle$. This is given by the spectral decomposition of ρ_P, where the spectral values are the weights

p_i. The eigenvalues of ρ_P read $(1 \pm s)/2$, and $s = ||\mathbf{s}||$, the length of the Bloch vector, is given by

$$s(\rho_P) = \left(\text{Tr}[\rho_P^2]\right)^{1/2} = \left(\sum_i \langle\sigma_i\rangle^2\right)^{1/2}. \qquad (7)$$

Hence, the entropy of entanglement can be expressed as

$$E(|\Psi\rangle) = h\left(\frac{1+s}{2}\right), \qquad (8)$$

where $h(x) = -x \log(x) - (1-x)\log(1-x)$ is the binary entropy. Note that s is a measure of mixedness of ρ_P and thus the vector nature of ρ in its own right. Optically, it corresponds to the degree of polarization of the averaged polarization state.

For incoherent vector beams with mixed states, the degree of mixedness (entropy) of the reduced density matrix can obviously not be directly used to determine the degree of the vector nature of the beam. While the notion of entanglement entropy E can be extended to mixed states, it is, in general, very difficult to calculate. An exception is a vector beam with only two orthonormal spatial modes populated. In this case the spatial degree of freedom and the polarization form a pair of two-level systems, and E can be determined for all mixed beam states by means of the concurrence C. In order to use the concurrence to determine the degree of the vector nature of a paraxial beam, the spatial degree of freedom has to be projected onto a two-dimensional subspace. This could, for example, be the space spanned by two Hermite-Gaussian or Laguerre-Gaussian modes and can be accomplished by using mode filters. In this regard we point out that, analogous to polarization states on the Poincaré sphere, we can depict orbital angular momentum (OAM) states of a reduced subspace on an equivalent sphere [40]. For example, the left- and right-handed helicities of the OAM states that lie on the poles of this sphere correspond to the left- and right-handed circularly polarized states on the Poincaré sphere (see Fig. 2). After this projection of the spatial degree of freedom, the elements of the resulting 4×4 beam coherence-polarization matrix can be detected by means of state tomography.

In the following we demonstrate experimental methods to measure the degree of the vector nature by means of state tomography and by detecting the degree of (averaged) polarization. Moreover, we introduce a third method that is based on measuring the violation of a Bell inequality.
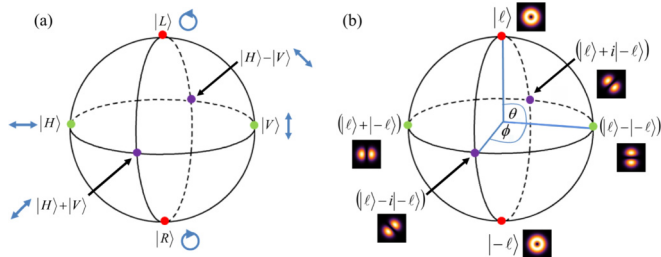
FIG. 2. (Color online) Bloch sphere representation of the degrees of freedom. (a) Bloch sphere representation for the states of polarization. (b) An analogous representation for orbital angular momentum states.

III. EXPERIMENTAL RESULTS

Our experimental setup can be seen in Fig. 3 and can be divided into two parts: the preparation of the vector beam and the measurement of its nonseparability. Without any loss of generality we have chosen to create vector vortex modes that lie on the higher-order Poincaré sphere.

We made use of a q plate [14] to prepare vector vortex modes. The q plate uses a spatially variant geometric phase to couple polarization to orbital angular momentum following the selection rules

$$|\ell, L\rangle \to |\ell + Q, R\rangle, \qquad (9)$$

$$|\ell, R\rangle \to |\ell - Q, L\rangle. \qquad (10)$$

The azimuthal charge introduced by the q plate is $Q = 2q$. The polarization distribution after the q plate depends on the initial incident polarization state. That is, horizontally polarized light will be transformed into a radially varying polarization state, while an azimuthally varying state is created from vertically polarized light incident on the q plate. In our experiment $q = 1/2$, and the incident Gaussian beam was horizontally polarized with $\ell = 0$, thereby generating a radially polarized vortex mode consisting of a superposition of $\ell = \pm 1$ modes. Thus, the field after the half-wave plate can be described by

$$|\Psi\rangle = \sqrt{a}|\ell=1\rangle|R\rangle \pm \sqrt{1-a}|\ell=-1\rangle|L\rangle, \qquad (11)$$

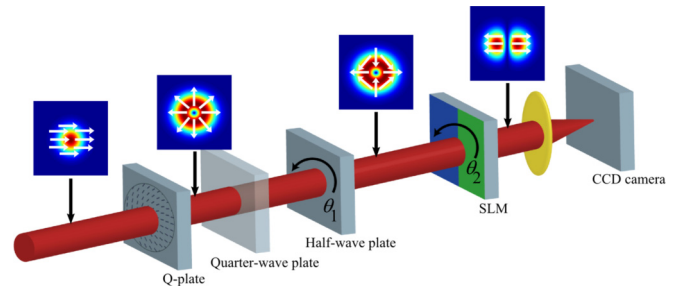where $|\ell = \pm 1\rangle$ represent the azimuthal components of the vortex beam.

FIG. 3. (Color online) Schematic representing the experimental procedure with which to generate and measure cylindrical vector (CV) beams. A horizontally polarized Gaussian beam incident on the q-wave plate is converted to a radially polarized vortex beam. The q plate converts left-handed circularly (LHC) polarized light into right-handed circularly (RHC) polarized light and adds OAM of $+1$ to the incident beam, while RHC is converted to LHC and OAM of -1 is added to the incident beam. Thus, the generated beam is a superposition of OAM modes, $|\ell = 1\rangle + |\ell = -1\rangle$, with radially varying polarization. A quarter-wave plate was inserted only to measure the circularly polarized modes and was set at an orientation of $\pi/4$ rad. The half-wave plate is then rotated by an angle θ_1, thereby measuring the polarization of the beam. The hologram encoded onto the SLM represents a superposition of OAM modes, $|\ell = 1\rangle + \exp(i\theta_2)|\ell = -1\rangle$, where θ_2 is the orientation of the hologram. The SLM, Fourier lens, and CCD camera together form the OAM-polarization detection component using a modal decomposition technique. The SLM directs horizontally polarized light into only the first diffraction order and therefore simultaneously acts as a polarizer while also performing an azimuthal decomposition.

To perform the necessary projections and state tomography we require only a wave plate and a spatial light modulator (SLM). In an entanglement setup, separate projections of the same property are performed simultaneously on a pair of entangled photons. For example, the polarization states are measured by placing a polarizer in the path of each photon, and the simultaneous arrival of the photons is recorded. Analogously, the OAM of each photon can be measured using SLMs as mode-specific filters. In the case of vector beams, both DOF must be measured locally: polarization and OAM. The measurement of states on the OAM subspace is performed by modal decomposition [24] using an SLM. In this experiment, we generated vortex modes carrying a superposition of OAM values $\ell = \pm 1$.

SLMs are also polarization sensitive in that the desired beam reflected from the screen consists of only horizontally polarized light. As such, the SLM acts as a horizontal polarizer, which, when rotated, acts as a filter for the linear polarization states: horizontal, vertical, diagonal, and antidiagonal. As a matter of practicality, we fixed the SLM to reflect only horizontally polarized light and instead inserted a half-wave plate before the SLM, which we rotate to realize a filter for the linear polarization states. By inserting an additional element, a quarter-wave plate, we were able to filter the circularly polarized components. The quarter-wave plate and rotation of the half-wave plate perform all the necessary projective measurements as outlined in the theory. After the modal decomposition of the input field u into the azimuthal modes

$\exp(i\ell\phi)$ such that $u = \sum_\ell a_\ell \exp(i\ell\phi)$, the modulus of the modal weighting coefficients a_ℓ can be determined by the inner product of the field with an azimuthal match filter. That is, $|\langle u | \exp(i\ell\phi)\rangle| = |a_\ell|$, which can be experimentally performed by directing the field u onto an SLM encoded with the match-filter hologram, $\exp(-i\ell\phi)$, and recording the on-axis intensity on a CCD camera after Fourier lens L_1 in Fig. 3. We used a HoloEye Pluto SLM with a resolution of 1080×1920 pixels and pixel size of 8 μm/pixel. The SLM was calibrated for a 2π phase shift at 633 nm [41].

We first performed a Clauser-Horne-Shimony-Holt-Bell (CHSH-Bell) inequality measurement [42] to demonstrate a violation of Bell's inequality using vector vortex modes. Typically, a CHSH-Bell inequality is performed on an entangled pair of photons and using a single degree of freedom, e.g., polarization [27] or OAM [43]. In our experiment, instead of measuring one degree of freedom nonlocally (e.g., two separated photons), we measure two DOF locally, i.e., on the same classical field. The CHSH-Bell parameter S satisfies the inequality $-2 \leqslant S \leqslant 2$ for classical correlations, in the case of entanglement, or for scalar beams, in the case of classical fields. We define the Bell parameter S as

$$S = E(\theta_1, \theta_2) - E(\theta_1, \theta_2') + E(\theta_1', \theta_2) + E(\theta_1', \theta_2'), \quad (12)$$

where $E(\theta_1, \theta_2)$ can be calculated by measuring the on-axis intensity $I(\theta_1, \theta_2)$ on the camera:

$$E(\theta_1, \theta_2) = \frac{I(\theta_1, \theta_2) + I\left(\theta_1 + \frac{\pi}{2}, \theta_2 + \frac{\pi}{2}\right) - I\left(\theta_1 + \frac{\pi}{2}, \theta_2\right) - I\left(\theta_1, \theta_2 + \frac{\pi}{2}\right)}{I(\theta_1, \theta_2) + I\left(\theta_1 + \frac{\pi}{2}, \theta_2 + \frac{\pi}{2}\right) + I\left(\theta_1 + \frac{\pi}{2}, \theta_2\right) + I\left(\theta_1, \theta_2 + \frac{\pi}{2}\right)}. \quad (13)$$

Here θ_1 and θ_2 are the angles of orientation of the half-wave plate and the encoded hologram, respectively. For each orientation of the wave plate, the holograms were rotated from $\theta_2 = 0$ to $\theta_2 = \pi$, and the on-axis intensity was recorded. This was repeated for four different orientations of the half-wave plate: $\theta_1 = 0$ rad, $\theta_1 = \pi/8$ rad, $\theta_1 = \pi/4$ rad, and $\theta_1 = 3\pi/8$ rad, as shown in Fig. 4. From Eqs. (12) and (13) we found our Bell parameter to be $S = 2.72 \pm 0.02$. We have demonstrated a violation of Bell's inequality by 36 standard deviations for these vector vortex modes. This highlights the nonseparability of the classical mode.

Next, we performed a full state tomography measurement to calculate the density matrix of the state, which we achieve by modifying existing tomography tools [28,44] to include both polarization and OAM. In this measurement we required not only the superposition states of polarization and OAM but also the pure states: left and right circular polarization and $\ell = \pm 1$ OAM modes. In terms of the higher-order Poincaré sphere, the pure modes are represented at the poles of the sphere. For each of the six polarization states (right, left, horizontal, diagonal, vertical, and antidiagonal), a modal decomposition was executed using six different holograms: $|\ell = 1\rangle$, $|\ell = -1\rangle$, $|\ell = 1\rangle + \exp(i\theta_2)|\ell = -1\rangle$ for $\theta_2 = 0, \pi/2, \pi, 3\pi/2$. Figure 5 shows the normalized intensity measurements for each of the six polarization states and the six OAM states.

This tomographic method produces an overcomplete set of 36 measurements, which can be used to minimize the χ^2 quantity and reconstruct the density matrix ρ. The degree of the vector nature of any field can then be calculated from the density matrix. We found the concurrence, a measure of
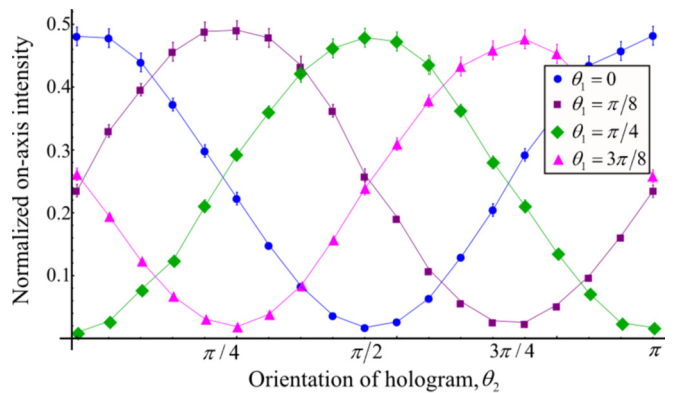

FIG. 4. (Color online) Bell-type curves for four different orientations of the half-wave plate. Orientations include $\theta_1 = 0$, $\theta_1 = \pi/8$, $\theta_1 = \pi/4$, and $\theta_1 = 3\pi/8$. For each change in polarization distribution, the hologram representing the superposition state $|\ell = 1\rangle + \exp(i\theta_2)|\ell = -1\rangle$ was rotated by $\theta_2 = \{0, \pi\}$ rad, and the on-axis intensity was recorded.
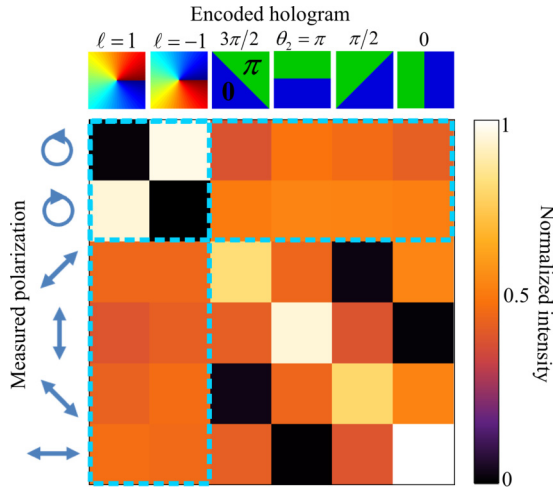
FIG. 5. (Color online) Experimental measurements obtained from a full state tomography measurement. The polarization was measured using a combination of a quarter-wave plate and half-wave plate. For each polarization state, the field was decomposed in the $\ell = |1|$ OAM basis, which includes both pure and superposition states, and the on-axis intensity was recorded. The measurements outlined by blue dashed lines were used to calculate the entanglement entropy of the vector beam, where either the pure OAM states (first two columns) or the circularly polarized states (first two rows) were chosen as the basis state.

the degree of the vector nature, of our vectorial field to be $C = 0.96 \pm 0.01$, while we found that of a scalar state to be $C = 0.09 \pm 0.01$. A maximal vector field is represented by 1, while a value of 0 represents a purely scalar field.

In fact, two states selected on the polarization (or OAM) sphere and projective measurements on the OAM (or polarization) are all that is required for the measurement of the entanglement entropy. This space within the full tomography measurements is shown within the dashed lines in Fig. 5. The purity r of the reduced density matrix in Eq. (7) was calculated by first selecting a spatial basis, e.g., the pure OAM states ($|\ell = \pm 1\rangle$) shown as the first two columns in Fig. 5, and then calculating the components of the Bloch vector. For example, $\langle \sigma_3 \rangle = \text{Tr}[(|R\rangle\langle R| - |L\rangle\langle L|)\rho_p] = \sum_{i=-1,1} |\langle l = i|u_R\rangle|^2 - |\langle l = i|u_L\rangle|^2$. Similar results are found for σ_1 and σ_2, where the horizontal and vertical states and the diagonal and antidiagonal states are considered, respectively. This resembles a degree of polarization measurement, and of course, any spatial basis can be chosen. However, the Poincaré and Bloch spheres in Fig. 2 clearly illustrate the analogy between polarization and an OAM subspace, and as such, we can also first choose a polarization basis, e.g., the circularly polarized states shown as the first two rows in Fig. 5, to calculate the purity r. Using Eq. (8), we calculated the entanglement entropy for the vector vortex beam to be 0.98 ± 0.01, which indicates a high level of nonseparability or vector nature. Table I compares the results of the three techniques for vector and scalar beams. We find that all the tools provide an accurate measure of the classical field and that in particular we are able to quantify the degree of the vector nature of the field.

TABLE I. Comparison between vector and scalar beams for three different measurements: a Bell inequality measurement, a concurrence measurement, and an entropy measurement. A Bell parameter greater than 2 represents a vector beam, while a value close to 1 for both the concurrence and entropy represents a vector beam. The errors for the scalar beam were insignificant.

	Bell parameter	Concurrence	Entropy
Vector	2.72 ± 0.02	0.96 ± 0.01	0.98 ± 0.01
Scalar	0.10	0.09	0.02

IV. DISCUSSION

In the 1990s statistical tools were applied to laser beam characterization and led to the now ubiquitous beam quality factor M^2 as a measure of modal content and divergence; here we provide a measure for the vector nature of classical fields through the use of quantum tools. It should be noted that this is a very practical tool: vector beams (for example, radially polarized beams) are now routinely used in applications such as laser materials processing, so a single measure of the quality of such beams could be of value to the community. The suitability of the quantum tools to this problem lies in the common property that vector beams share with entangled states: nonseparability. In some sense these fields may be considered akin to entangled states, and hence, the phrase "classical entanglement" has emerged [34,36,45–47]. But we stress that while these fields are nonseparable in polarization and spatial modes, they are not entangled in the quantum sense; one would not extend the nonseparability property to nonlocality or nonrealism (there is no unique reality before measurement). But it is interesting to ask whether such fields may be used to mimic quantum processes in which only the nonseparability property is required. Such fields may then be applicable as vehicles to realize quantum processes such as quantum random walks [48] as well as tripartite quantum states [39].

V. CONCLUSION

Using measurement techniques more commonly associated with quantum entanglement, we have demonstrated methods to distinguish between scalar and vector beams and to determine the degree of nonseparability, or vector nature, of the vector beam. We find that the entanglement entropy is a proxy for the average degree of polarization and thus provides a single number for the vector nature of such beams. We envisage that such tools will find practical use in applications in which such beams are routinely used.

APPENDIX A: ACTION OF THE HALF-WAVE PLATE

The spatial light modulator (SLM) acts on only the horizontally polarized component of a beam. As such, if the SLM is rotated, it will act on the different states of polarization. The rotation of the half-wave plate in the experimental setup is equivalent to rotating the SLM, as the half-wave plate changes the polarization state of the beam and the SLM thereafter acts on the horizontal component. A half-wave plate can be written

as a Jones matrix as follows:

$$
\begin{pmatrix} \cos(2\theta) & \sin(2\theta) \\ \sin(2\theta) & -\cos(2\theta) \end{pmatrix},
\tag{A1}
$$

where θ is the angle between the fast axis and the horizontal axis. By setting $\theta = 0$ rad, the polarization of a field u is transformed as

$$
\begin{pmatrix} u_x \\ u_y \end{pmatrix} \xrightarrow{0 \text{ rad}} \begin{pmatrix} u_x \\ -u_y \end{pmatrix}.
\tag{A2}
$$

As the SLM acts on only the horizontal component of the field, we see that we measure the original horizontal component. However, if the plate is rotated such that $\theta = \pi/4$ rad, then we measure the vertical component of the original beam.

$$
\begin{pmatrix} u_x \\ u_y \end{pmatrix} \xrightarrow{\pi/4 \text{ rad}} \begin{pmatrix} u_y \\ u_x \end{pmatrix}.
\tag{A3}
$$

Similarly, the diagonal and antidiagonal polarization components can be measured by orientating the plate at $\theta = \pi/8$ rad and $\theta = 3\pi/8$ rad, respectively. This is seen in Eqs. (A4) and (A5).

$$
\begin{pmatrix} u_x \\ u_y \end{pmatrix} \xrightarrow{\pi/8 \text{ rad}} \frac{1}{\sqrt{2}} \begin{pmatrix} u_x + u_y \\ u_x - u_y \end{pmatrix},
\tag{A4}
$$

$$
\begin{pmatrix} u_x \\ u_y \end{pmatrix} \xrightarrow{3\pi/8 \text{ rad}} \frac{1}{\sqrt{2}} \begin{pmatrix} -u_x + u_y \\ u_x + u_y \end{pmatrix}.
\tag{A5}
$$

Thus, using the half-wave plate together with the polarization-sensitive SLM, each polarization state along the equator of the Poincaré sphere can be measured.

APPENDIX B: ACTION OF THE QUARTER-WAVE PLATE

A quarter-wave plate was inserted between the q plate and half-wave plate in Fig. 3 to measure the circular polarization states of the vector beam. The Jones matrix for a quarter-wave plate is written as

$$
\begin{pmatrix} \cos^2\theta + i\sin^2\theta & \sin\theta\cos\theta - i\sin\theta\cos\theta \\ \sin\theta\cos\theta - i\sin\theta\cos\theta & \sin^2\theta + i\cos^2\theta \end{pmatrix}.
\tag{B1}
$$

Again, θ is the angle between the fast axis of the plate and the horizontal axis. Setting the plate at an orientation with $\theta = \pi/4$, the Jones matrix becomes

$$
\frac{\exp(i\pi/4)}{\sqrt{2}} \begin{pmatrix} 1 & -i \\ -i & 1 \end{pmatrix}.
\tag{B2}
$$

Thus, the action of a quarter-wave plate orientated at $\theta = \pi/4$ on a field u is described by

$$
\begin{pmatrix} u_x \\ u_y \end{pmatrix} \xrightarrow{\pi/4 \text{ rad}} \frac{\exp(i\pi/4)}{\sqrt{2}} \begin{pmatrix} u_x - iu_y \\ -u_x + u_y \end{pmatrix}.
\tag{B3}
$$

Thus, looking at only the horizontal component, the quarter-wave plate allows us to measure right-circularly polarized light. If the half-wave plate is oriented at either $\theta = 0$ or $\theta = \pi/4$, we can measure right- or left-circularly polarized light, respectively.

APPENDIX C: CONCURRENCE

The entanglement entropy E can be determined for all mixed beam states by means of the concurrence C:

$$
E(\rho) = h\left(\frac{1 + \sqrt{1 - C^2}}{2} \right).
\tag{C1}
$$

Because of the one-to-one correspondence between C and E, the concurrence represents an alternative entanglement measure for pairs of two-level systems. It is given by

$$
\mathcal{C}(\rho) = \max\{0, \sqrt{\lambda_1} - \sqrt{\lambda_2} - \sqrt{\lambda_3} - \sqrt{\lambda_4}\},
\tag{C2}
$$

with λ_i being the eigenvalues in decreasing order of the Hermitian matrix

$$
R = \rho(\sigma_y \otimes \sigma_y)\rho^*(\sigma_y \otimes \sigma_y),
\tag{C3}
$$

where the asterisk (*) represents the complex conjugate and σ_y is the Pauli y matrix,

$$
\sigma_y = \begin{bmatrix} 0 & -i \\ i & 0 \end{bmatrix}.
\tag{C4}
$$

[1] C. E. R. Souza, J. A. O. Huguenin, P. Milman, and A. Z. Khoury, Phys. Rev. Lett. **99**, 160401 (2007).

[2] Q. Zhan, Adv. Opt. Photonics **1**, 1 (2009).

[3] L. Novotny, M. R. Beversluis, K. S. Youngworth, and T. G. Brown, Phys. Rev. Lett. **86**, 5251 (2001).

[4] Q. Zhan, Opt. Express **12**, 3377 (2004).

[5] A. F. Abouraddy and K. C. Toussaint, Phys. Rev. Lett. **96**, 153901 (2006).

[6] X. Li, T.-H. Lan, C.-H. Tien, and M. Gu, Nat. Commun. **3**, 998 (2012).

[7] B. Roxworthy and K. Toussaint, New J. Phys. **12**, 073012 (2010).

[8] D. Pohl, Appl. Phys. Lett. **20**, 266 (1972).

[9] F. Enderli and T. Feurer, Opt. Lett. **34**, 2030 (2009).

[10] T. Grosjean, D. Courjon, and M. Spajer, Opt. Commun. **203**, 1 (2002).

[11] R. Zheng, C. Gu, A. Wang, L. Xu, and H. Ming, Opt. Express **18**, 10834 (2010).

[12] W. Han, W. Cheng, and Q. Zhan, Opt. Lett. **36**, 1605 (2011).

[13] C. Maurer, A. Jesacher, S. Fürhapter, S. Bernet, and M. Ritsch-Marte, New J. Phys. **9**, 78 (2007).

[14] L. Marrucci, C. Manzo, and D. Paparo, Phys. Rev. Lett. **96**, 163905 (2006).

[15] S. Slussarenko, A. Murauski, T. Du, V. Chigrinov, L. Marrucci, and E. Santamato, Opt. Express **19**, 4085 (2011).

[16] F. Cardano, E. Karimi, S. Slussarenko, L. Marrucci, C. de Lisio, and E. Santamato, Appl. Opt. **51**, C1 (2012).

[17] G. Milione, H. I. Sztul, D. A. Nolan, and R. R. Alfano, Phys. Rev. Lett. **107**, 053601 (2011).

[18] A. Holleczek, A. Aiello, C. Gabriel, C. Marquardt, and G. Leuchs, Opt. Express **19**, 9714 (2011).

[19] F. Töppel, A. Aiello, C. Marquardt, E. Giacobino, and G. Leuchs, New J. Phys. **16**, 073019 (2014).

[20] J. W. Nicholson, A. D. Yablon, S. Ramachandran, and S. Ghalmi, Opt. Express **16**, 7233 (2008).

[21] O. Shapira, A. F. Abouraddy, J. D. Joannopoulos, and Y. Fink, Phys. Rev. Lett. **94**, 143902 (2005).

[22] H. Lü, P. Zhou, X. Wang, and Z. Jiang, Appl. Opt. **52**, 2905 (2013).

[23] D. Flamm, D. Naidoo, C. Schulze, A. Forbes, and M. Duparré, Opt. Lett. **37**, 2478 (2012).

[24] I. Litvin, A. Dudley, F. Roux, and A. Forbes, Opt. Express **20**, 10996 (2012).

[25] G. Stokes, Trans. Cambridge Philos. Soc. **96**, 399 (1852).

[26] A. Dudley, G. Milione, R. Alfano, and A. Forbes, Opt. Express **22**, 14031 (2014).

[27] A. Aspect, P. Grangier, and G. Roger, Phys. Rev. Lett. **47**, 460 (1981).

[28] B. Jack, J. Leach, H. Ritsch, S. Barnett, and M. J. Padgett, New J. Phys. **811**, 103024 (2009).

[29] W. K. Wootters, Quantum Inf. Comput. **1**, 27 (2001).

[30] E. Karimi, J. Leach, S. Slussarenko, B. Piccirillo, L. Marrucci, L. Chen, W. She, S. Franke-Arnold, M. J. Padgett, and E. Santamato, Phys. Rev. A **82**, 022115 (2010).

[31] C. V. S. Borges, M. Hor-Meyll, J. A. O Huguenin, and A. Z. Khoury, Phys. Rev. A **82**, 033833 (2010).

[32] K. Kagalwala, G. Di Giuseppe, A. Abouraddy, and B. Saleh, Nat. Photonics **7**, 72 (2013).

[33] A. Luis, Opt. Commun. **282**, 3665 (2009).

[34] C. Gabriel, A. Aiello, W. Zhong, T. Euser, N. Joly, P. Banzer, M. Förtsch, D. Elser, U. Andersen, C. Marquardt *et al.*, Phys. Rev. Lett. **106**, 060502 (2011).

[35] R. J. C. Spreeuw, Found. Phys. **28**, 361 (1998).

[36] R. J. C. Spreeuw, Phys. Rev. A **63**, 062302 (2001).

[37] S. Goyal and T. Konrad, in *Laser Beam Propagation: Generation and Propagation of Customized Light*, edited by A. Forbes (CRC Press, Boca Raton, FL, 2014), pp. 41–75.

[38] F. Gori, M. Santarsiero, S. Vicalvi, R. Borghi, and G. Guattari, Pure Appl. Opt. **7**, 941 (1998).

[39] A. Aiello, F. Toeppel, C. Marquardt, E. Giacobino, and G. Leuchs, New J. Phys. **17**, 043024 (2015).

[40] M. J. Padgett and J. Courtial, Opt. Lett. **24**, 430 (1999).

[41] J. Davis and I. Moreno, in *Laser Beam Propagation: Generation and Propagation of Customized Light*, edited by A. Forbes (CRC Press, Boca Raton, FL, 2014), pp. 175–236.

[42] J. F. Clauser, M. A. Horne, A. Shimony, and R. A. Holt, Phys. Rev. Lett. **23**, 880 (1969).

[43] J. Leach, B. Jack, M. Ritsch-Marte, R. Boyd, A. Jha, S. Barnett, S. Franke-Arnold, and M. J. Padgett, Opt. Express **17**, 8287 (2009).

[44] M. Agnew, J. Leach, M. McLaren, F. S. Roux, and R. W. Boyd, Phys. Rev. A **84**, 062101 (2011).

[45] B. N. Simon, S. Simon, F. Gori, M. Santarsiero, R. Borghi, N. Mukunda, and R. Simon, Phys. Rev. Lett. **104**, 023901 (2010).

[46] X.-F. Qian and J. Eberly, Opt. Lett. **36**, 4110 (2011).

[47] P. Ghose and A. Mukherjee, Rev. Theor. Sci. **2**, 274 (2014).

[48] S. K. Goyal, F. S. Roux, A. Forbes, and T. Konrad, Phys. Rev. Lett. **110**, 263602 (2013).